Nano Energy 53 (2018) 383–390

Contents lists available at ScienceDirect

Nano Energy

journal homepage: www.elsevier.com/locate/nanoen

Full paper

Triboelectric charge density of porous and deformable fabrics made from polymer fibers

Shirui Liu[a], Wei Zheng[a,b], Bao Yang[a], Xiaoming Tao[a,*]

[a] Nanotechnology Centre for Functional and Intelligent Textiles and Apparel, Institute of Textiles and Clothing, Hong Kong Polytechnic University, Hong Kong, China
[b] Sunsong (Shenzhen) Polymer Eco-Friendly New Material Co.,Ltd., Shenzhen, China

ARTICLE INFO

Keywords:
Triboelectrification
Triboelectric series
Charge density
Porous materials
Contact area

ABSTRACT

Triboelectricity has attracted much attention for its potential applications in harvesting mechanical energy by triboelectric nanogenerators, whose output performance is dominated by triboelectric charge density. The number of electric charges generated on interactive surfaces is an intrinsic property of the materials directly related to their chemical structure and high-order structures. This paper deals with a sliding-mode triboelectrification system and measurement methods of the charge density on highly porous and deformable materials like textile fabrics with a structural hierarchy. Effects of operational parameters of the system, structures and properties of fabrics made from twenty one types of polymer fibers were investigated. It is found that the effective charge density of fabrics can be reliably measured when the tribo-electrification process reaches its saturation under the fabric densification pressure. An extended table of measured tribo-electric charge density is compiled with highly porous and deformable knitted fabrics made from twenty one types of polymer fibers.

1. Introduction

Recently, triboelectricity has been widely explored as a mean of harvesting mechanical energy for wearable and self-powered electronic [1–7]. Fibrous structures like textile fabrics have demonstrated great flexibility and outstanding fatigue resistance, apart from other advantages, in such wearable application [8–12]. More specifically, in triboelectric nanogenerator [13–16], soft, deformable or porous polymeric materials are utilized, such as textile fabrics made from Polytetrafluoroethylene (PTFE), Polydimethylsiloxane (PDMS), Polyvinyl chloride (PVC) etc. [17–20]. Triboelectrification of interactive surfaces is one of the two main mechanisms for triboelectric nanogenerators. Previous theoretical and experimental studies have revealed that the surface charge density is the most important factor determining the output performance of such nanogenerators [21,22]. An in-situ method was reported to quantitatively characterize nanoscale triboelectrification of relatively smooth films, by utilizing a combination of contact-mode AFM and scanning Kevin probe microscopy (SKPM). This method could precisely control the contact force, area, speed, and cycles of the triboelectric process, provide information on triboelectric charge spatial distribution, multifriction effect, and the subsequent charge diffusion on the dielectric surface [23].

In general, the number of electric charges generated on the interactive surface is an intrinsic property of a material directly related to its chemical structure and, to some degree, its high-order structures [24]. The areal charge density is influenced by the morphology of the interactive surface area. As pointed by Lowell and Rose-Innes [25], it is meaningless to compare the absolute charge density values obtained from various tests in the previous report works, since the real contact area was not controlled thus varied for different materials under different testing conditions. A rough and questionable estimation was made by them that the real contact area was about half of the apparent contact area (geometric contact area). For instance, the measured surface charge density of PTFE film was reported as 0.7 nC/cm^2 [21], much lower than the theoretical value predicted at the saturated state of the material (2.97 nC/cm^2). Many similar studies did not confirm whether the number of charges of the materials had reached the saturated state, and the testing condition was not illustrated clearly [26–29]. Some materials like textile fabrics are very deformable and porous, thus the previous measurements cannot provide reliable data of absolute charge density of materials despite the existence of the triboelectric series. Therefore, it is much desirable to improve the current experimental methods for triboelectric charge density by considering the charge saturation and effects of structural characteristics of the deformable and porous materials like fabrics.

Sliding contact has been the desirable approach to conduct the tribo-electrification experiments. It allows the transfer of triboelectric charges and materials between two solids, for whose mechanisms are

* Corresponding author.
E-mail address: xiao-ming.tao@polyu.edu.hk (X. Tao).

https://doi.org/10.1016/j.nanoen.2018.08.071
Received 21 July 2018; Received in revised form 30 August 2018; Accepted 30 August 2018
Available online 31 August 2018

elusive. Several researchers provided a number of explanations, including an increase in contact area due to interfacial deformation, frictional heating and direct material transfer. For instance, measurements of sliding electrification versus normal force carried out by Wåhlin and B¨ackstr¨om [30] suggested that interfacial deformation was dominant in the system of Teflon on metal. Bowden and Tabor [31] proposed that intense localized frictional heating promoted charge transfer. Some tribo-electrification experiments with metals in the “dry severe wear” regime (e.g. Chang et al. [32]) illustrated the significant role played by material transfer. Many effects are undetermined such as surface morphology and compressibility, variations in experimental methods, the nature of contact, uncertainty as to the transferred charge species and the effect of charge back-flow.

In this study, the electron charge density of porous and deformable textile fabrics made from a range of polymeric fibers is measured by utilizing a lab-made sliding-mode tribo-electrification measurement system. An optical fabric tribological meter is employed, by using fiber Bragg grating sensing and laser triangulation method, to measure the surface morphology and friction of textile fabrics. The effects of fabric surface roughness, friction coefficient. The compression caused change in contact area is taken into consideration when deriving the effective charge density. A extended table of measured effective charge density is compiled to cover various fabrics made from twenty one types of polymer fibers. The results of this basic research will shed light on the triboelectric behavior of new polymer fibers and their textile fabrics. They will also support fundamental research to better understand mechanisms associated with electrostatic charge generation and transfer via the linkage between theories and practical applications.

2. Sliding-mode triboelectrification measurements

2.1. Measurement setup

A sliding-mode triboelectrification measurement system was set up and employed to perform sliding test of the fabrics, collect and measure triboelectric charges. It is consisted of two instruments. Universal tensile tester Instron 5944 is attached with a device that provides the sliding motion with a controlled speed. It has a copper sliding track board, a driver unit, a copper block, the data acquisition and control unit, as shown in Fig. 1a. A nylon filament is connected the front of the copper block of 400 g, which is pulled through a pulley fixed on the metal track board, held by the upper cramp of Instron 5944, with a speed of 750 mm/min. The second instrument is a Nano-coulomb Meter connected with a faraday tube to measure the electric charge of samples, as shown in Fig. 1b. During the test, the copper track board is connected with the earth all the time.

2.2. Sample preparation

Single jersey knitted fabrics were made from twenty one types of polymeric filaments and staple yarns by TRICOLAB cylinder hosiery machine with knitting gauge 22, 3 fabric samples for each yarn. Before the measurements, all the prepared fabric samples were washed (ISO 6330–2012) for 30 mins at the 40 ± 2 °C by using non-ionic detergent Diadavin EWN, 200%, 2 g/L with a liquor ratio of 60:1, and then dried naturally and balanced for 24 h in standard conditions 22 °C, 65% RH in paper bags. As a pretreatment, the initial residual charges on the samples were neutralized by one metal board connected with the earth.

Single jersey knitted fabric samples of 30 mm in width and 120 mm in length were laid lightly on the copper block of 30 mm x 120 mm x 20 mm and fixed by adhesive tapes, and the face side in the wale direction of fabric samples was chosen as the interactive surface to be rubbed with the copper track board, since the effective contact area of face side (with more loop legs) is larger than the back side (with more loop sinkers), as shown in Fig. 1c, d, and in the wale direction, the loop shape is more stable than that in the course direction of the single jersey knitted fabrics in the sliding process.

2.3. Operation conditions

Careful considerations were given to select appropriate testing conditions so that the samples reached their equilibrium number of charges and variations of measurements could be minimized. The pressure of 1.6 KPa was chosen as at this value, fabric samples will reach and go beyond the fabric densification threshold. Sliding speed of 750 mm/min was used for all tests. Another important consideration is

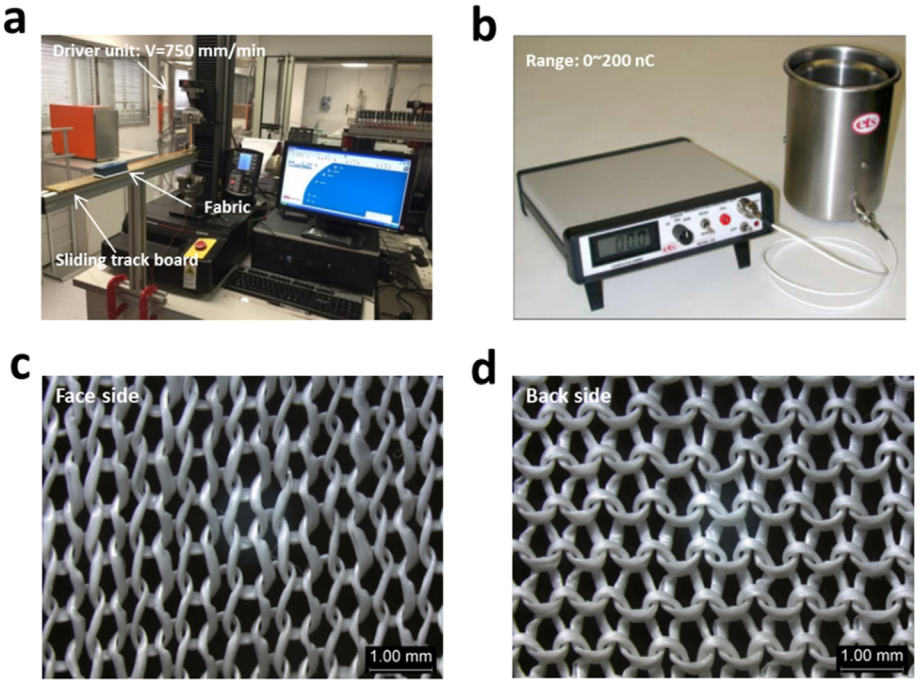

Fig. 1. (a) Instron 5944 and sliding meter. (b) Nano-coulomb Meter (Model: 230). (c) Face side of single jersey knitted fabric. (d) Back side of single jersey knitted fabric.

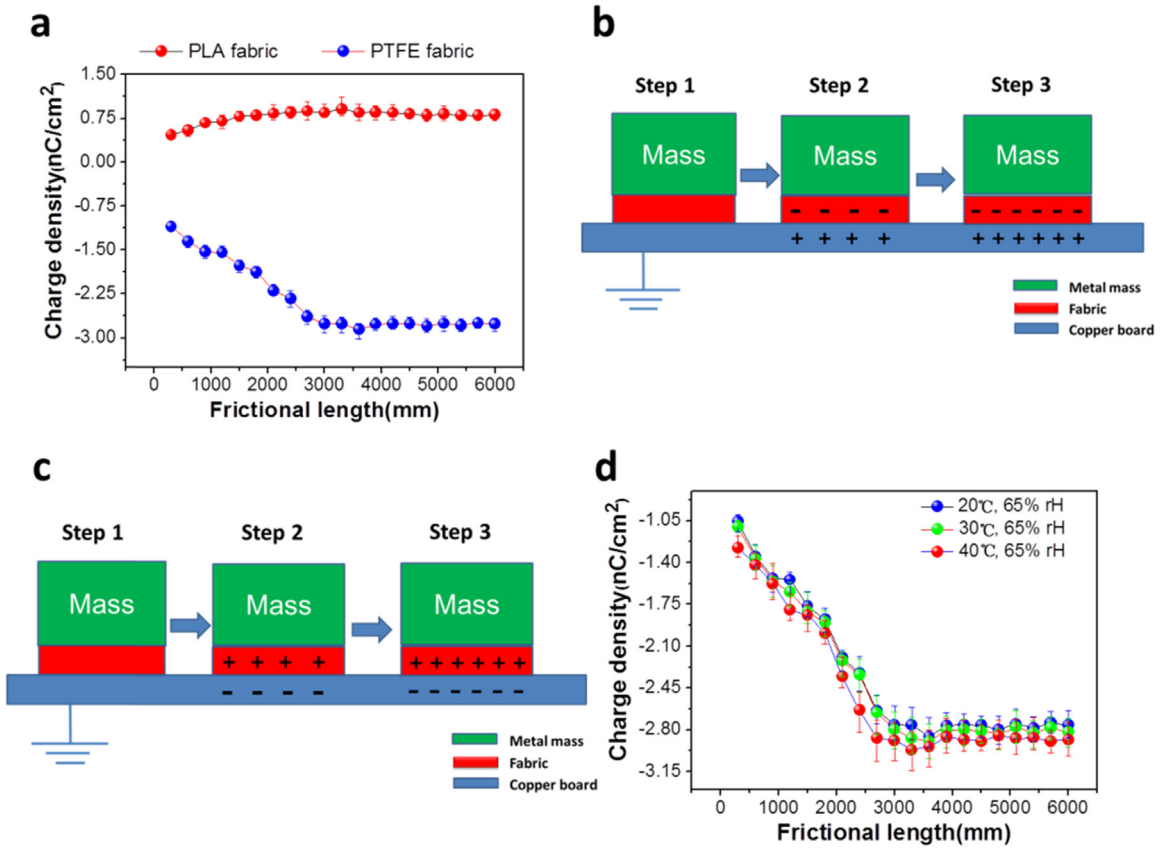

Fig. 2. (a) Effective charge density of PTFE and PLA fabrics plotted as a function of sliding length. (b) Sliding process of negative-charged material against copper board. (c) Sliding process of positive-charged material against copper board. (d)Effective charge density of PTFE fabrics sliding against copper board at various temperatures.

the sliding distance. Fig. 2a shows the effective charge density of PTFE (negative) and PLA (positive) fabrics plotted against the sliding distance. During the sliding process, the charge amount generated increased from the beginning then reached a relative plateau status. Therefore it was very important to conduct the measurement when the number of charges reached its saturation.

The charge density increases sharply at the beginning and then reaches a stable state with increasing sliding distance, which is mainly due to the charge accumulation and saturation as limited by the surface area of fabric sample. The sliding distance in the measurement was then selected as 6 m for all measurements of charge density.

Fig. 2b depicts that the tribo-electrification and electrostatic induction process of negative-charged fabric samples rubbed with a copper track board. The process can be divided into 3 stages, that is, the initial stage, followed up by sliding stage and finally stage of charge saturation. The electrostatic charge generation of the fabric samples works under the collective effects by tribo-electrification and electrostatic induction. In the initial stage, there is no electrostatic charge as the fabric and copper board have cleared out all residual charges. During the sliding stage, the fabric gains the negative charges due to the property of material itself while the metal track board has equal positive charges, as the metal easily loses the electrons to the fabric. In the finally stage, the charge of fabric sample has reached saturation, the interactive surfaces, that is, the bottom of the fabric and the upper of the metal board have opposite static charges (tribo-charges) respectively with equal numbers. Fig. 2c demonstrates that the process of positive-charged fabric sample sliding against copper board. Compared with Fig. 2b, the fabric sample obtained positive charges when sliding on the copper track board. As a result of electrostatic induction, the copper board would gain the negative charges.

The effect of temperature variation is presented in Fig. 2d. The PTFE fabrics and the sliding-mode triboelectrification measurement system were placed in the Floor-standing Temperature and Climatic Test Chamber (Model: C7–600) for conditioning for two hours at a given temperature, meanwhile the humidity was controlled at 65% RH. Each test was conducted for 20 cycles. When one sliding cycle was completed, the electric charge of samples was measured by the Nano-coulomb Meter connected with a faraday tube. Fig. 2d clearly shows that the charge density of PTFE fabric increases slightly when the temperature changes from 20 °C to 40 °C. The reason is due to enhancement of electron activity of copper and the dielectric material at elevated temperature, and more electrons lost from the copper. When reaching saturation, the charge densities of PTFE fabrics are kept at a relative stable value.

3. Measurement and effects of fabric surface roughness

In order to identify the effect of fabric surface roughness on charge density, two techniques were applied. Laser triangulation sensor (Model: Microtrak™-LTS 25-04) was set up and employed to obtain 3D mapping of the fabric surface. The sensor had digital resolution: 0.076 μm; laser angle 45 ; Spot size: 30 μm; measurement range: 4 mm. It was mounted on the front mobile platform of the Automatic Surface Tester (KESFB4-AUTO-A , KATO TECH CO., LTD), as shown in Fig. 3. The sensor's head was adjusted to the top of the sample platform.

Each sample was measured three times in each principle. Based on the values of thickness measured, the mean deviations from mean thickness (SMD), or surface roughness, were derived by:

$$\mathrm{SMD} = \frac{1}{X}\int_0^X |T - \bar{T}|dx \quad (1)$$

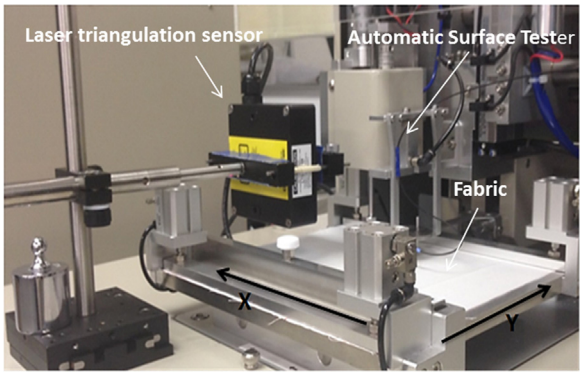

Fig. 3. Surface mapping unit.

where $X = 3$ cm, T is thickness of the specimen at position x and $\bar{T}$ is mean value of T.

Alternatively, an optical measurement system (Alicona IFM G4) was utilized with scanning time of 4.0–6.6 s and 3 times / sample.

Three PTFE knitted fabrics made from the same yarn were used in the investigation. They have various fabric densities in the course direction from 30 to 35 courses/in and a fixed wale density of 37 wales/inch. Fig. 4a shows that fabric 1 has a higher roughness than fabric 2 and 3 in the wale direction. When the roughness increases, the charge density derived with nominal contact area arises significantly, as shown in Fig. 4b. However, when the effective contact area is used for the charge density derivation, the effect of roughness becomes much reduced, close to none.

4. Measurement and effect of fabric surface friction coefficient

The next question is the effect of friction on the charge density of the fabrics. We employed a highly sensitive tactile sensor made from optic fiber Bragg gratings (FBG) and PDMS [33]. As shown in Fig. 5a, two single-mode silica optic fibers with Bragg gratings were embedded into a soft PDMS cube in the horizontal and titled direction, respectively. The central wavelength of fiber Bragg grating was 1553 nm and the dimension of the tube was 2.5 cm x 2.5 cm x 2.5 cm. The tactile sensor was connected with optical sensing interrogator (Micro optics sm130). The calibrated curves of the peak wavelength shifts of the horizontal FBG (hFBG) and titled FBG (tFBG) under normal and frictional loadings are given by [33]

$$\Delta\lambda_{hFBG} = 36.8P_n - 26.5P_s \ (R^2 = 0.986) \quad (2)$$

$$\Delta\lambda_{tFBG} = 19.3P_n + 50.3P_s \ (R^2 = 0.992) \quad (3)$$

where, $\Delta\lambda_{hFBG}$ is the peak wavelength shift of hFBG (pm), $\Delta\lambda_{tFBG}$ is the peak wavelength shift of hFBG (pm), P_n is the applied normal stress on silicone cube (kPa); P_S is the applied shear stress on silicone cube (kPa); R^2 is values of correlation coefficient.

The frictional coefficients, μ, of the PTFE knitted fabrics were obtained by

$$\mu = \frac{Ps}{Pn} \quad (4)$$

Fig. 5b shows that PTFE fabric 1 and 2 are similar as to have a relative higher pressure and sheer stress than that of PTFE fabric 3. The nominal and effective charge densities of the three fabrics decrease with the increment of frictional coefficient. However, the changes due to the variation in frictional coefficient becomes insignificant when the effective charge density is concerned, which further demonstrates indirectly that the effective contact area is the most critical factor affecting charge density of deformable and porous fabrics. In practical energy harvesting applications in other modes than contact mode, where densification is not guarented, the variation in friction coefficient may cause a significant effect on the surface charge density.

5. Measurement and effect of fabric contact area

5.1. Effective surface contact area

Up to now, we have demonstrated that the surface roughness and friction coefficient of the fabrics have little influence on the effective charge density calculated from the effective contact area. Fabric is porous and soft, easily deformed thus contact area varies significantly under compression. Thus the effective contact area of the fabrics under compression was obtained in the following manner. Eighteen PTFE knitted fabrics and eighteen PTFE films with 30 mm x 120 mm were chosen. Inkpad and Cartesian paper were adopted for recording by counting the number of color points on the paper. Five metal plates of 100 g, 200 g, 300 g, 400 g and 500 g were selected as compression loads. A sample with the back side attached on the metal plate was placed on the inkpad under its weight. The ink on the fabric face was transferred to a Cartesian paper by stamping finally. The image of the contact area was analyzed by a digital image analysis system using correlation analysis (ImageJ). The effective contact area is given then by

$$Se = \oint dA = N\alpha = N\left(\frac{L_0}{P_0}\right)^2 \quad (5)$$

where S_e is the effective contact area of textiles, A is the nominal contact area of materials, N is the total number of pixels of effective contact area, α represents the actual area size of each pixel, the

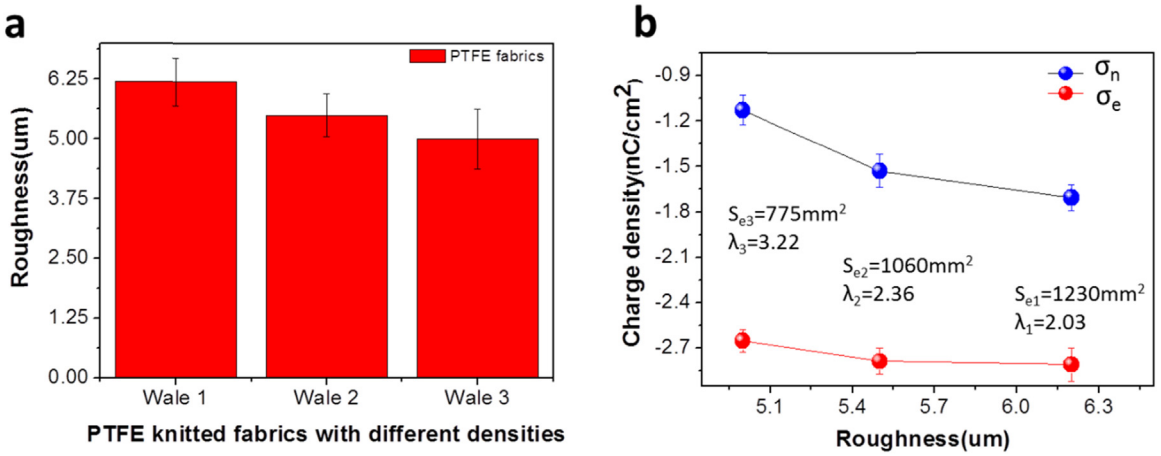

Fig. 4. (a) Roughness of PTFE knitted fabrics with various densities. (b) Charge densities of PTFE knitted fabrics in the wale direction.

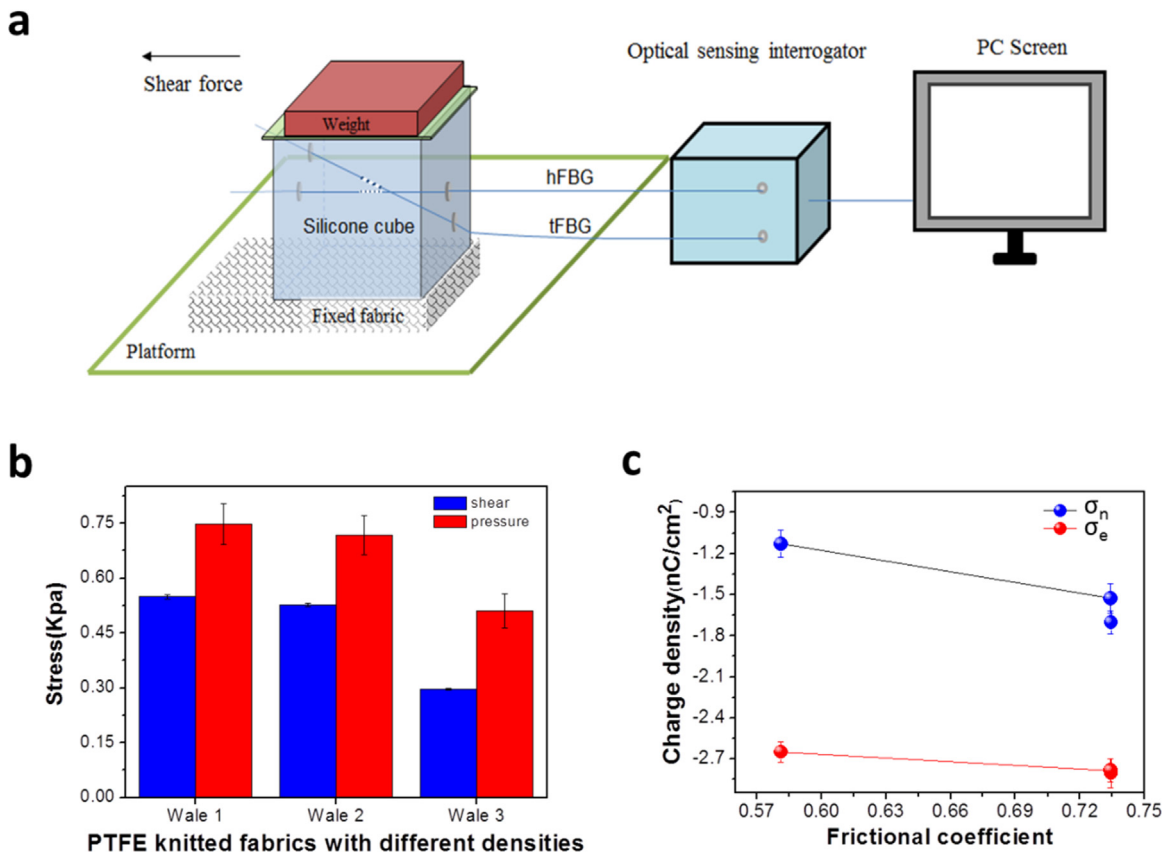

Fig. 5. (a) Schematic diagram of friction unit. (b) Stress of PTFE knitted fabrics with different densities. (c) Charge densities of fabrics plotted against frictional coefficient.

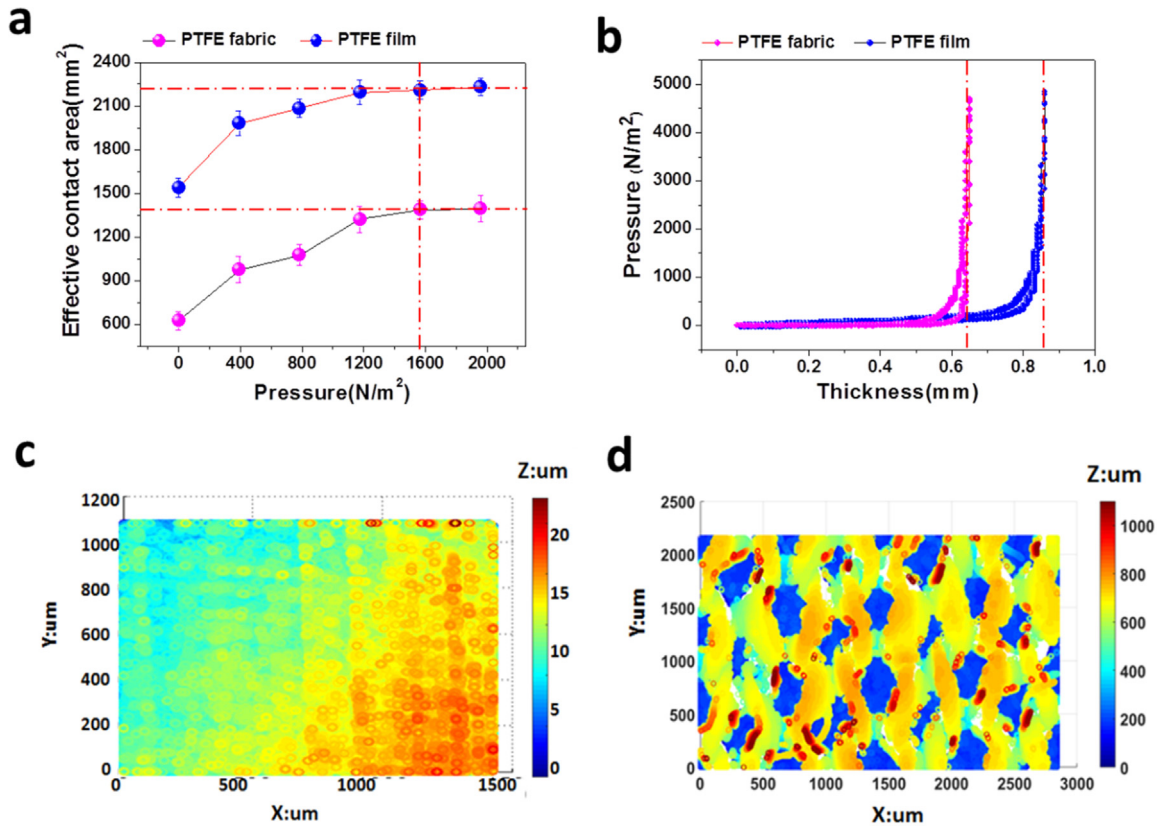

Fig. 6. (a) Effective contact areas of PTFE textile materials with different weights of metals. (b) Pressure-thickness curves of PTFE film and PTFE fabric. (c) Surface profile of PTFE film and (d) Surface profile of PTFE fabric obtained by 3D optical measurement (Alicona IFM G4).

calibration distance L_0, and the corresponding pixels P_0.

Fig. 6a shows the effective contact areas of PTFE fabrics and films under different pressures. The contact area of PTFE film is larger than that of the PTFE fabric, and the contact areas for both increase with increasing pressure. When the pressure reaches a critical value of 1600 N/m^2, the PTFE film and fabric obtain relative steady values of thickness when the initial porous structure becomes dense so that all fibers are in contact with each other. Further compression is to compress fibers. The compression curves in Fig. 6b depict that when the pressure reaches 1600 N/m^2, the thickness of PTFE fabric and PTFE film is 0.65 mm and 0.85 mm, respectively. They reach the core thickness, which could obtain the biggest effective contact area. In other word, many surface and internal features disappear under the densification pressure. Moreover, the PTFE film is stiffer and has less space to be compressed than the PTFE fabric, illustrated by the slope difference as shown in Fig. 6b. It is vital to obtain the maximum effective contact area of fabrics under a pressure at which the densification of fabric occurs. Compared with other fabrics used, the stiffness of the PTFE fabric is relative higher , therefore the pressure 1600 N/m^2 was selected to conduct the sliding-triboelectric tests of fabrics in their densification region in order to obtain highest contact area.

Fig. 6c and d illustrate the digitized images of a compressed PTFE film and a fabric, respectively. Both samples were subject to the densification pressure of 1600 N/m^2. The effective contact area of the film is larger than the fabric. The fabric has many bigger pores on the surface. It has an effective area of 1371 mm^2 and nominal area of 2500 mm^2, the coefficient of proportionality, the ratio of effective contact area and nominal area, $\lambda = 1.82$, while the film is 1.13.

5.2. Effective charge density σ_e

It takes consideration of the number of charges measured and the effective surface contact area, as described below:

$$\sigma_e = \frac{Q}{A}\lambda = \frac{\sum_{i=k}^{n} q_i}{nA}\lambda \,(\mathrm{n} = \mathrm{k},\ \mathrm{k}+1,\ \mathrm{k}+2\ldots) \tag{6}$$

where Q is the number of charges measured after the saturation is reached, A is the nominal contact area of the sample, n is sliding times, λ is the coefficient of proportionality, the ratio between the effective contact area and the nominal area, k is the point of the saturation value obtained, q_i is charge of the sample each time after it reaches saturation.

5.3. Effect of pressure

The large variation in measured charge density with pressure is demonstrated in Fig. 7a for both the film and fabric samples, which is associated with the change in the actual contact area under compression. The charge density reaches maximum when the pressure reaches densification value of 1600 N/m^2, and both the film and fabric present a similar trend with pressure. When the pressure increases, the effective charge density increases first, arrives at the maximum value and then reduced. This phenomenon may be brought by the fact that the pressure results in the increasing effective contact areas to assist to reach saturation. However, when the number of charges is in saturation, further increasing pressure is useless as the effective contact area has been used fully. It is not clear why there are decreases of the charge when the pressure is greater than the densification value of 1600 N/m^2, although one may suggest occurrence of materials transfer after the saturation.

The results also provide useful insight when fabrics are used for other modes of triboelectric energy harvesting. Two important effects may occur, that is, the densification of interfacing yarns due to deformation, and the yarn residual stress which gives a rise of localized denstification due to manufacturing processes. Hence, one need to consider them when design and fabricate the energy harvesting fabrics.

5.4. Implication of the effective charge density

Fig. 7(b) clearly illustrates that the charge density of PTFE fabric is very close to that of film if the effective area is used under the densification pressure of 1600 N/m^2. For instance, the PTFE fabric has the measured negative charge density of -2.75 nC/cm^2, close to the theoretical value predicted from bulk PTFE (-2.97 nC/cm^2) [21]. In other word, the effective charge density of the fabrics obtained are very close to the intrinsic charge density of the polymer materials that constitute the fabrics, while the effects of fiber, yarn and fabric structures are largely eliminated by the proposed measurement methods.

6. Charge densities of fabrics and triboelectric series

The measured effective charge density of various kinds of fabrics and their specifications are shown in Table 1. Our results on the fabrics show the huge differences between the change density values using nominal and effective contact areas. The difference is 77% for PTFE and 81% for PLA, significantly higher than the previous estimation of 50% change in contact area [25]. Therefore it is essential to consider the effective contact area under compression when measuring the charge density of porous and deformable materials like fabrics.

The table illustrates the very significant variations of the charge density values measured by difference groups [21,24–28]. For instance, the reported value varies from -0.020 to -3.000 nC/cm^2 for PTFE. In our work, the PTFE fabric has the highest negative charge density of -2.75 nC/cm^2, much closer to the theoretical value predicted at the

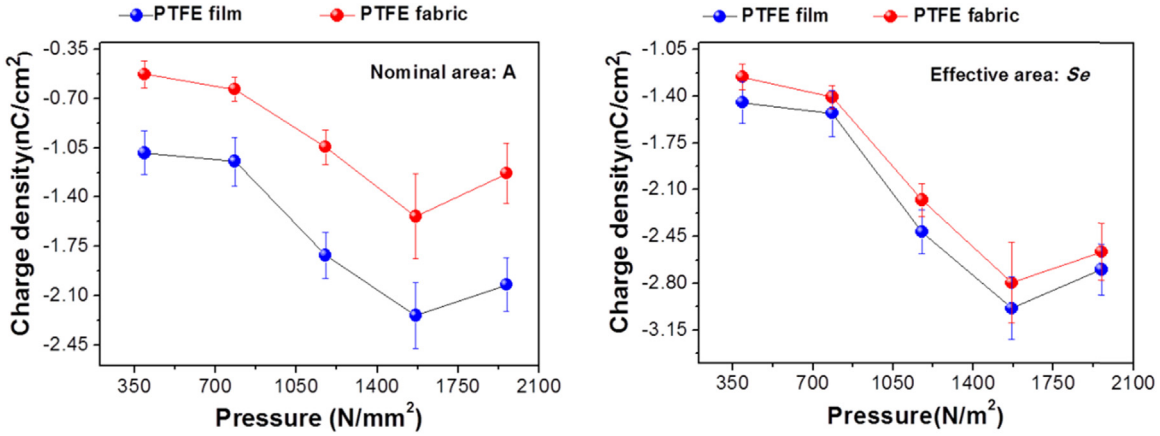

Fig. 7. Charge density of PTFE fabric and film plotted against compressional load by using (a) nominal area, and (b) effective area obtained from the digital image analysis (ImageJ).

Table 1
Measured charge densities of single jersey knitted fabrics and materials.

Fiber materials	Yarn speciation	Effective charge density nC/cm^2 (CV)	Nominal charge density nC/cm^2 (CV)	Reported charge density nC/cm^2 [21,25–29]
Polytetrafluoroethylene (PTFE)	210D	**−2.750** (23.00%)	−1.550 (14.00%)	−0.020, −0.700, −3.000
Polyethylene (PE)	210D/48f	**−1.260** (11.20%)	−0.900 (7.30%)	−0.001, −0.015, −0.500
Polyimide (PI)	210D/48f	**−0.473** (2.30%)	−0.370 (4.50%)	−0.001
Polypropylene (PP)	20Ne	**−0.312** (12.50%)	−0.230 (3.46%)	−0.001
Polyparaphenylene terephthalamide (Kevlar)	210D/108f	**−0.112** (3.46%)	−0.070 (2.45%)	Nil
Polyethylene terephthalate (PET)	210D/108f	**−0.109** (4.50%)	−0.067 (3.56%)	−0.001
Polyacrylonitrile (PAN)	32Ne	**−0.065** (2.45%)	−0.045 (4.51%)	0.00039
Cotton	32Ne	**0.011** (2.30%)	0.005 (2.45%)	0.0012–0.0015,
Ramie	32Ne	**0.029** (1.39%)	0.010 (2.34%)	0.0012–0.0015
Beta-poly- D-glucosamine (Chitosan)	32Ne	**0.034** (4.32%)	0.016 (4.55%)	Nil
Fiberglass	180D/108f	**0.105** (4.56%)	0.055 (3.52%)	Nil
Wool	32Ne	**0.142** (3.43%)	0.068 (1.34%)	0.005–0.009
Cuprammonuium (Cupro)	75D/48f	**0.159** (2.38%)	0.079 (3.45%)	Nil
Lyocell (Cellulose fiber)	75D/48f	**0.163** (1.33%)	0.081 (2.41%)	Nil
Polycaprolactam (Nylon 6)	210D/108f	**0.283** (2.40%)	0.150 (4.65%)	0.005–0.009
Silk	32Ne	**0.342** (4.56%)	0.180 (3.44%)	0.005–0.009
Polyurethane	40D	**0.385** (9.84%)	0.200 (4.45%)	0.005–0.009
Poly[imino(1,6-dioxohexamethylene)iminohexamethylene](Nylon 66)	210D/108f	**0.422** (5.55%)	0.230 (5.66%)	0.005–0.009
Poly(3-hydroxybutyrate-co − 3-hydroxyvalerate) (PHBV)	75D/48f	**0.453** (3.56%)	0.240 (6.74%)	Nil
Polylactide/Poly(3-hydroxybutyrate-co − 3-hydroxyvalerate) (PLA/PHBV)	75D/48f	**0.643** (4.24%)	0.320 (6.73%)	Nil
Polylactide (PLA)	75D/48f	**0.872** (3.56%)	0.480 (3.57%)	Nil

Notes: D stands for denier, linear density in g/9 km; f is the number of fiber; and Ne is the English yarn count, the length of 770 m in 0.45 kg.

saturated state (−2.97 nC/cm^2) as compared with previous measured values [21,24–28]. On the other end, PLA fabric exhibits the highest positive value of + 0.81 nC/cm^2. Fabrics made from natural cellulose fibers like cotton, ramie, wool and chitosan show the lowest values of approximately + 0.01 nC/cm^2, with silk as an exception. Unlike aromatic polyesters like polyethylene terephthalate, aliphatic polyesters like PLA, PHBV and PHBV/PLA all have high values of positive charge density. The results extend the existing triboelectric series as several new fibrous materials are added including PHBV, PLA, Lyocell, and Cupro.

7. Conclusion

This paper presents a new measurement method of effective charge density of porous and highly deformable materials like textile fabrics. A sliding-mode tribo-electrification measurement system is described. The effects on the measured charge density by its operation parameters, e.g. pressure and sliding distance, are determined with optimal operation conditions. The influences of structural characteristics of the fabrics are investigated including friction coefficient, surface roughness, compressibility and contact area under the densification pressure. Among all these structural factors, the effective surface area under densification pressure has been identified as the most critical and important factor. The measurement thus leads to the values close to the intrinsic charge density of the bulk materials regardless the complex structural hierarchy.

This paper compiles a table of measured tribo-charge densities of fabrics made from twenty one types of polymer fibers, some are included for the first time. Moreover, the charge density of all these fabrics are obtained in the saturated and densification states, which will provide reliable data in the search for best performing functional materials for triboelectric nano-generators.

Acknowledgements

This work is supported by the Research Grants Council of Hong Kong,China (Project No. 525113, 15215214, 15211016E, 15200917)

References

[1] X. Pu, L. Li, H. Song, C. Du, Z. Zhao, C. Jiang, G. Cao, W. Hu, Z.L. Wang, A self-charging power unit by integration of a textile triboelectric nanogenerator and a flexible lithium-ion battery for wearable electronics, Adv. Mater. 27 (2015) 2472–2478, https://doi.org/10.1002/adma.201500311.
[2] J. Lee, H. Kwon, J. Seo, S. Shin, J.H. Koo, C. Pang, S. Son, J.H. Kim, Y.H. Jang, D.E. Kim, Sensors: conductive fiber-based Ultrasensitive textile pressure sensor for Wearable Electronics (Adv. Mater. 15/2015), Adv. Mater. 27 (2015) 2409, https://doi.org/10.1002/adma.201570100.
[3] H. Chu, H. Jang, Y. Lee, Y. Chae, J.-H. Ahn, Conformal, graphene-based triboelectric nanogenerator for self-powered wearable electronics, Nano Energy 27 (2016) 298–305, https://doi.org/10.1016/j.nanoen.2016.07.009.
[4] J. Kim, J. Lee, D. Son, M.K. Choi, D.-H. Kim, Deformable devices with integrated functional nanomaterials for wearable electronics, Nano Converg. 3 (2016) 4, https://doi.org/10.1186/s40580-016-0062-1.
[5] A.M. Hussain, F.A. Ghaffar, S.I. Park, J.A. Rogers, A. Shamim, M.M. Hussain, Wearable Electronics: metal/polymer based Stretchable antenna for constant frequency far-field communication in Wearable Electronics (Adv. Funct. Mater. 42/2015), Adv. Funct. Mater. 25 (2015) 6557, https://doi.org/10.1002/adfm.201570269.
[6] Q. Zheng, H. Zhang, B. Shi, X. Xue, Z. Liu, Y. Jin, Y. Ma, Y. Zou, X. Wang, Z. An, In vivo self-powered wireless cardiac monitoring via implantable triboelectric nanogenerator, ACS Nano 10 (2016) 6510–6518, https://doi.org/10.1021/acsnano.6b02693.
[7] S. Hong, H. Lee, J. Lee, J. Kwon, S. Han, Y.D. Suh, H. Cho, J. Shin, J. Yeo, S.H. Ko, Highly stretchable and transparent metal nanowire heater for wearable electronics applications, Adv. Mater. 27 (2015) 4744–4751, https://doi.org/10.1002/adma.201500917.
[8] L. Zhang, S. Lin, T. Hua, B. Huang, S. Liu, X. Tao, Fiber-based thermoelectric generators: materials, device structures, fabrication, characterization, and applications, Adv. Energy Mater. 8 (2018) 1700524, https://doi.org/10.1002/aenm.201700524.
[9] S. Chen, X. Tao, W. Zeng, B. Yang, S. Shang, Quantifying energy harvested from contact-mode hybrid nanogenerators with cascaded piezoelectric and triboelectric units, Adv. Energy Mater. 7 (2017), https://doi.org/10.1002/aenm.201601569.
[10] W. Zeng, X.-M. Tao, S. Chen, S. Shang, H.L.W. Chan, S.H. Choy, Highly durable all-fiber nanogenerator for mechanical energy harvesting, Energy Environ. Sci. 6 (2013) 2631–2638, https://doi.org/10.1039/C3EE41063C.
[11] J. Song, B. Yang, W. Zeng, Z. Peng, S. Lin, J. Li, X. Tao, Highly flexible, large-area, and facile textile-based hybrid nanogenerator with cascaded piezoelectric and triboelectric units for mechanical energy harvesting, Adv. Mater. Technol. (2018) 1800016, https://doi.org/10.1002/admt.201800016.
[12] X. Tao, Handbook of Smart Textiles, Springer, Singapore, 2015.
[13] S. Chen, N. Wang, L. Ma, T. Li, M. Willander, Y. Jie, X. Cao, Z.L. Wang, Triboelectric nanogenerator for sustainable wastewater treatment via a self-powered electrochemical process, Adv. Energy Mater. 6 (2016), https://doi.org/10.1002/aenm.201501778.
[14] K. Zhang, X. Wang, Y. Yang, Z.L. Wang, Hybridized electromagnetic–triboelectric nanogenerator for scavenging biomechanical energy for sustainably powering wearable electronics, ACS Nano 9 (2015) 3521–3529, https://doi.org/10.1021/nn507455f.
[15] C. Xue, J. Li, Q. Zhang, Z. Zhang, Z. Hai, L. Gao, R. Feng, J. Tang, J. Liu, W. Zhang, A novel arch-shape nanogenerator based on piezoelectric and triboelectric mechanism for mechanical energy harvesting, Nanomaterials 5 (2014) 36–46, https://doi.org/10.3390/nano5010036.

[16] T. Quan, X. Wang, Z.L. Wang, Y. Yang, Hybridized electromagnetic–triboelectric nanogenerator for a self-powered electronic watch, ACS Nano 9 (2015) 12301–12310, https://doi.org/10.1021/acsnano.5b05598.
[17] F.-R. Fan, L. Lin, G. Zhu, W. Wu, R. Zhang, Z.L. Wang, Transparent triboelectric nanogenerators and self-powered pressure sensors based on micropatterned plastic films, Nano Lett. 12 (2012) 3109–3114, https://doi.org/10.1021/nl300988z.
[18] G. Zhu, C. Pan, W. Guo, C.-Y. Chen, Y. Zhou, R. Yu, Z.L. Wang, Triboelectric-generator-driven pulse electrodeposition for micropatterning, Nano Lett. 12 (2012) 4960–4965, https://doi.org/10.1021/nl302560k.
[19] G. Zhu, Z.-H. Lin, Q. Jing, P. Bai, C. Pan, Y. Yang, Y. Zhou, Z.L. Wang, Toward large-scale energy harvesting by a nanoparticle-enhanced triboelectric nanogenerator, Nano Lett. 13 (2013) 847–853, https://doi.org/10.1021/nl4001053.
[20] G. Zhu, J. Chen, Y. Liu, P. Bai, Y.S. Zhou, Q. Jing, C. Pan, Z.L. Wang, Linear-grating triboelectric generator based on sliding electrification, Nano Lett. 13 (2013) 2282–2289, https://doi.org/10.1021/nl4008985.
[21] S. Niu, Y. Liu, S. Wang, L. Lin, Y.S. Zhou, Y. Hu, Z.L. Wang, Theory of sliding-mode triboelectric nanogenerators, Adv. Mater. 25 (2013) 6184–6193, https://doi.org/10.1002/adma.201302808.
[22] B. Yang, W. Zeng, Z. Peng, S. Liu, K. Chen, X. Tao, A. Fully, Verified theoretical analysis of contact-mode triboelectric nanogenerators as a wearable power source, Adv. Energy Mater. 6 (2016), https://doi.org/10.1002/aenm.201600505.
[23] Y.S. Zhou, Y. Liu, G. Zhu, Z.-H. Lin, C. Pan, Q. Jing, Z.L. Wang, In situ quantitative study of nanoscale triboelectrification and patterning, Nano Lett. 13 (2013) 2771–2776, https://doi.org/10.1021/nl401006x.
[24] H.T. Baytekin, A.Z. Patashinski, M. Branicki, B. Baytekin, S. Soh, B.A. Grzybowski, The mosaic of surface charge in contact electrification, Science 333 (80) (2011) 308–312, https://doi.org/10.1126/science.1201512.
[25] J. Lowell, A.C. Rose-Innes, Contact electrification, Adv. Phys. 29 (1980) 947–1023, https://doi.org/10.1080/00018738000101466.
[26] D. Truncyte, M. Gutauskas, S. Zebrauskas, J. Virbalis, Triboelectricity in the pairs of polymeric materials, J. Appl. Polym. Sci. 110 (2008) 3532–3537, https://doi.org/10.1002/app.28926.
[27] J. Lowell, A.R. Akande, Contact electrification-why is it variable? J. Phys. D Appl. Phys. 21 (1988) 125, https://doi.org/10.1088/0022-3727/21/1/018.
[28] E.M. Charlson, E.J. Charlson, S. Burkett, H.K. Yasuda, Study of the contact electrification of polymers using contact and separation current, IEEE Trans. Electr. Insul. 27 (1992) 1144–1151, https://doi.org/10.1109/14.204865.
[29] A.F. Diaz, R.M. Felix-Navarro, A semi-quantitative tribo-electric series for polymeric materials: the influence of chemical structure and properties, J. Electrost. 62 (2004) 277–290, https://doi.org/10.1016/j.elstat.2004.05.005.
[30] A. Wåhlin, G. Bäckström, Sliding electrification of teflon by metals, J. Appl. Phys. 45 (1974) 2058–2064, https://doi.org/10.1063/1.1663545.
[31] F.P. Bowden, D. Tabor, The Friction and Lubrication of Solids, Clarendon, Oxford, 1954.
[32] Y.-P. Chang, Y.-C. Chiou, R.-T. Lee, Tribo-electrification mechanisms for dissimilar metal pairs in dry severe wear process: part I. Effect of speed, Wear 264 (2008) 1085–1094, https://doi.org/10.1016/j.wear.2007.03.008.
[33] Z.F. Zhang, X.M. Tao, H.P. Zhang, B. Zhu, Soft fiber optic sensors for precision measurement of shear stress and pressure, IEEE Sens. J. 13 (2013) 1478–1482, https://doi.org/10.1109/JSEN.2012.2237393.

Shirui Liu received the B.S. degree (2007) in Textile Engineering at University of Dezhou, China. He obtained the M.S. degree (2010) at Donghua University with a major research on Textile Engineering. He is now a Research Associate of Prof. Tao Xiaoming at Institute of Textiles and Clothing, the Hong Kong Polytechnic University. His research mainly focuses on the triboelectricity, novel spinning technologies and green bio-based degradable antibacterial textiles.

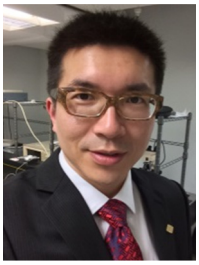

Wei Zheng received the Ph.D. degree (2014) at Institute of Textiles and Clothing, the Hong Kong Polytechnic University. He is now the R&D director in Sunsong (Shenzhen) Polymer Eco-Friendly New Material Co.,Ltd.. His research focused on the functional and degradable film, flexiable display technology and wearable technology.

Bao Yang obtained a B.Eng. (2007) in Engineering Mechanics and a Ph.D. (2012) in Solid Mechanics from South China University of Technology. Then he joined Prof. Tao group as a postdoc fellow at Institute of Textile and Clothing, the Hong Kong Polytechnic University. Major fields of research are wearable electronics and photonics, energy harvesting technology, impact dynamics, and structural design.

Xiaoming Tao is Chair Professor of Textile Technology, Institute of Textiles and Clothing, The Hong Kong Polytechnic University since 2002. She is the founding Director of Research Center of Smart Wearable Technology. She obtained a B.Eng. in Textile Engineering from East China Institute of Textile Science and Technology with a 1st class prize and a Ph.D. in Textile Physics from University of New South Wales in Australia. Prof. Tao is former World President from 2007 to 2010, Fellow of the Textile Institute, Fellow of American Society of Mechanical Engineering.